Received: 31 October 2022 | Revised: 12 January 2023 | Accepted: 18 February 2023

DOI: 10.1002/jcc.27099

RESEARCH ARTICLE

Journal of COMPUTATIONAL CHEMISTRY WILEY

Implementation of probe rheology simulation technique in atomistically detailed molecular dynamics simulations

Pouria Nourian | Andrew J. Peters

Chemical Engineering Department, Louisiana Tech University, Ruston, Louisiana, USA

Correspondence
Andrew J. Peters, Chemical Engineering Department, Louisiana Tech University, Ruston, LA 71270, USA.
Email: apeters@latech.edu

Abstract

The probe rheology simulation technique is a technique for measuring the viscosity of a fluid by measuring the motion of an inserted probe particle. This approach has the benefit of greater potential accuracy at a lower computational cost than other conventional simulation techniques used for the calculation of mechanical properties, such as the Green–Kubo approach and nonequilibrium molecular dynamics simulations, and the potential to allow for sampling local variations of properties. This approach is implemented and demonstrated for atomistically detailed models. The viscosity of four different simple Newtonian liquids is calculated from both the Brownian motion (passive mode) and the forced motion (active mode) of an embedded probe particle. The probe particle is loosely modeled as a nano-sized diamond particle: a rough sphere cut out of an FCC lattice made of carbon atoms. The viscosities obtained from the motion of the probe particle are compared with those obtained from the periodic perturbation method, and good agreement between the two sets of values is observed once the probe-fluid interaction strength (i.e., ϵ_{ij} in the pair-wise Lennard–Jones interaction) is two times higher than their original values, and the artificial hydrodynamic interactions between the probe particle and its periodic images are accounted for. The success of the proposed model opens new opportunities for applying such a technique in the rheological characterization of local mechanical properties in atomistically detailed molecular dynamics simulations, which can be directly compared with or help guide experiments of similar nature.

KEYWORDS
atomistic, molecular dynamics, probe rheology, rheology, viscosity

1 | INTRODUCTION

Microrheology, or probe rheology, is a recently developed but powerful tool for rheological characterization of various soft matter materials.[1–8] In microrheology, the viscoelastic properties of soft matter can be extracted from either the thermal (in passive mode) or forced (in active mode) motion of an embedded nano or micron-sized probe particle. The particle's motion is probed through various optical techniques[9–15] and related to the material's mechanical properties through the generalized Langevin equation. Microrheology requires only small amounts of sample, can expand the accessible frequency range compared with conventional methods, and can theoretically be used to probe the local variations in viscoelastic properties.[2] However, the studies regarding the simulation equivalent of microrheology are scarce, despite the fact that the validity of the Stokes' law and the Stokes–Einstein (SE) relation, which underly said technique, have been demonstrated in molecular dynamics (MD) simulations.[9–13,16] The two major issues hindering the widespread application of probe rheology in simulations until recently have been (1) choice of simulation parameters needed for robust implementation of this technique in the simulations, especially in active mode, have not been comprehensively analyzed, and (2) artificial hydrodynamic interactions (AHIs) among

the probe particle and its periodic images, arising from the use of periodic boundary conditions (PBCs) in the simulations with finite box sizes, can quantitively affect the trajectory of the probe particle motion, and result in substantial errors in the calculation of mechanical properties (which usually manifest as an overprediction of the said properties[14]).

Probe rheology simulation technique (PRST) is a recently developed MD simulation approach analogous to microrheology. PRST has been successfully implemented for coarse-grained models of polymer melts.[15,17,18] The conditions for the successful implementation of the technique in the active mode in coarse-grained simulation have been identified,[15] the issue of the finite simulation box size and its effect on the accessible frequency range and simulation cost has recently been addressed, and a modification to the underlying formulation of the technique has been proposed to take into account the effect of such interaction on the calculation of mechanical properties.[14] Similar work has been done on rheological characterization of coarse-grained entangled polymer melts by Ge et al.,[19] although they have used multiples particles in the system (with the volume fraction of the particles being ~10%), which is different than the previously mentioned PRST studies, which all employed a single probe particle.

The benefits of using PRST for the calculation of mechanical properties in simulations are twofold: (1) PRST can be more accurate and less computationally expensive compared with other conventional simulations techniques used for the calculation of mechanical properties such as the Green–Kubo (GK) approach and nonequilibrium molecular dynamics (NEMD) simulations,[14] and (2) PRST allows for the calculation of local mechanical properties. In the GK approach, based on the Onsager regression hypothesis,[20] the viscosity is obtained from the time integral of the stress autocorrelation function.[21,22] However, due to the accumulation of noise,[23] the stress autocorrelation term will often fluctuate even after long simulation runs. As a result, the time integral will either not reach a stationary value or have significant statistical uncertainties. In the NEMD method, oscillatory shear is applied to the simulation box through a modified equation of motion and the sliding-brick PBCs,[24,25] and the viscosity is calculated from the resulting stress. Several NEMD simulations at varying shear rates are required to extrapolate the zero-shear viscosity, which can be computationally expensive to obtain depending on the relaxation time of the system.

Second, all the conventional simulation techniques that calculate mechanical properties can only obtain the properties of the bulk by design. PRST, however, probes only the local properties in the vicinity of the probe particle. Thus, PRST can be used to calculate local mechanical properties, a valuable feature when designing novel materials. For example, thermoset shape memory polymers (TSMPs) are of particular interest in various industries due to their ability to recover their original shape under the effect of external stimuli.[26,27] The TSMP will soften but not melt when heated due to the chemical crosslinking throughout the material.[28] This procedure results in variations in the crosslinked structure (that is, the topology) and, consequently, different mechanical properties within different regions of the material. Measuring these variations in mechanical properties, possible when using PRST, would provide valuable insight into the fundamentals of TSMP behavior.

However, to the best of our knowledge, the PRST has only been applied to coarse-grained models thus far. The motivation for this work is to extend the application of PRST to atomistically detailed MD simulations. The major challenge for implementing the PRST in atomistically detailed simulations is the determination of probe-fluid interaction parameters. In the original coarse-grained implementation, PRST uses a rough probe particle, that is, a probe particle made up of a collection of beads and thus, has a rough surface. Moreover, the probe-fluid interaction is tuned to be stronger than the fluid–fluid interactions to ensure the satisfaction of the no-slip boundary condition at the surface of the probe particle; otherwise, the hydrodynamic boundary coefficient of 6 in the Stokes' law is no longer valid due to partial or perfect slip being present at the probe-fluid interface. Therefore, one must calculate the appropriate hydrodynamic boundary coefficient using the slip length, which is challenging. We propose a similar model for the probe particle in the atomistically detailed simulations: a sphere cut out of an FCC lattice made of carbon atoms. Such a model can be thought of as a diamond nanoparticle with adjustments to the particle-fluid interaction parameters. For the model to be universal, we need to understand how the probe-fluid interactions must be manipulated to ensure the satisfaction of the no-slip boundary condition.

We first describe the relations used for obtaining the viscosity from the Brownian or the forced motion of the probe particle, focusing on detailing the importance of having the no-slip boundary condition at the surface of the probe particle, as well as how these relations were modified to account for the AHIs. We then systematically study the relationship between the probe-fluid interaction strength and the obtained viscosities from both the passive and the active modes in different fluids to elucidate the universality of the proposed parameters for the model.

2 | METHODOLOGY

2.1 | Viscosity calculation from the motion of a probe particle

The viscosity of a fluid can be calculated from either the diffusion coefficient of the probe particle undergoing Brownian motion using the SE relation (Equation 1) when the motion of the particle is diffusive or from the velocity of a probe undergoing steady motion under the effect of a constant applied force (similar to a falling or rolling ball viscometer[29]) using Stokes' law (Equation 2):

$$D = \frac{k_B T}{c\pi\eta R_H}, \tag{1}$$

$$F = c\pi\eta v R_H, \tag{2}$$

where D is the diffusion coefficient, R_H is the particle's hydrodynamic radius, T is the temperature, k_B is the Boltzmann constant, η is the

viscosity, and c is the hydrodynamic boundary condition coefficient,[12,13] mentioned previously.

Theoretically, c can have a value between 4 and 6, depending on the extent of slip at the particle surface. A value of $c = 4$ corresponds to the perfect slip boundary condition (i.e., no shear stress being exerted at the particle surface by the fluid). On the opposite extreme, a value of $c = 6$ corresponds to the stick/no-slip boundary condition (i.e., the fluid velocity on the particle surface is the same as the surface velocity, and the shear stress exerted on the particle surface is proportional to the velocity gradient). Both the perfect slip and stick boundary conditions are ideal scenarios. A more generalized boundary condition, known as the Navier–Maxwell-Basset boundary condition, takes into account some degree of slip by hypothesizing that there is a finite slip velocity at the surface which is proportional to the surface shear stress. In this context, the slip length (L_s) is the depth (below the solid surface) at which the extrapolated velocity of the fluid and surface velocity are the same. Thus, perfect slip corresponds to an infinite L_s, whereas the no-slip corresponds to $L_s = 0$. A modified Stokes' law can be derived using the Navier–Maxwell-Basset boundary condition, thus allowing the hydrodynamic boundary condition coefficient to be directly related to the slip length as follows:

$$c = 6\left[\frac{\frac{R}{L_s}+2}{\frac{R}{L_s}+3}\right]. \tag{3}$$

Although Equation (3) allows for the direct calculation of c in the case of partial slip being present at the particle surface, such a calculation is a cumbersome task and requires that L_s would also be determined. Instead, the probe particle is modeled such that the no-slip boundary condition holds. Previous MD simulations of smooth (i.e., single bead) and rough (i.e., made up of a collection of beads) probe particles in LJ solvent have shown that at the surface of a smooth particle that is weakly interacting with the medium, slip boundary condition holds. By contrast, the stick boundary condition is applicable for a rough particle strongly interacting with the medium.[12,13,30,31] Thus, a rough probe particle was used, and the probe-fluid interaction strength was tuned to ensure that the no-slip boundary condition holds at the probe particle surface. In these previous simulations, the best results were achieved when the particle's bare radius was not used for R_H, but instead the distance from the particle's center of mass to the first solvation shell in the particle-fluid radial distribution ($g(r)$) plot.[12,13,30] The hydrodynamic radius of the particle differs from its bare radius by approximately the solvent radius[12,13,30]; thus, it is prudent to use the R_H in simulations where the probe particle is not much larger than the solvent particles.

Finally, Stokes' law and the SE relation are based on continuum mechanics; thus, they are applicable only when the moving probe particle perceives the medium as a continuum, that is, when the probe particle size is greater than the largest characteristic length scale of the medium. The breakdown of SE predictions observed in experiments[32–36] and simulations[37–40] can be attributed to a failure of the continuum approximation. Thus, it must be made sure that the probe particle is larger than the characteristic length scale of the medium, which for a simple Newtonian fluid, is the molecule size (more specifically, the radius of gyration of the molecules).

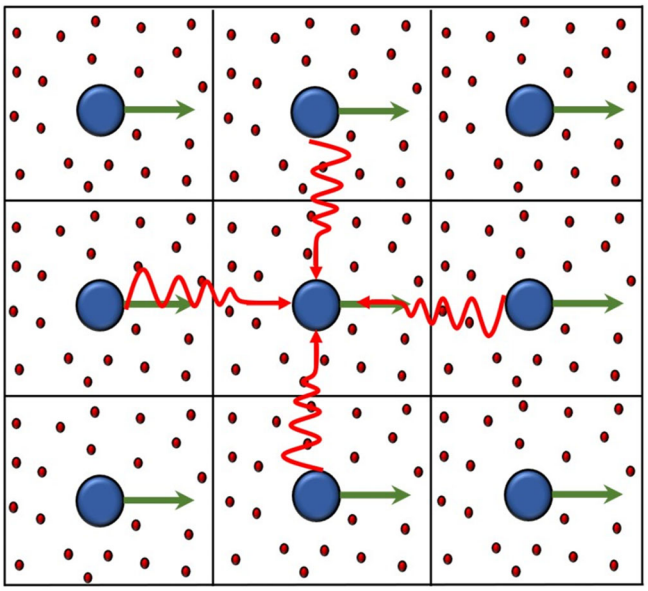

FIGURE 1 Schematic of motion of an array of particles caused by periodic boundary conditions and the resulting artificial hydrodynamics interactions. Reprinted with permission from reference [15]. Copyright 2021, Society of Rheology

2.2 | Hydrodynamic correction factor

As mentioned earlier, as a result of using PBCs in MD simulations, the particle and its periodic images can interact with each other through the so-called AHIs, which can adversely affect the trajectory of the probe particle motion and are a significant source of error in the calculation of mechanical properties when using the PRST. The AHIs have two components: the unsteady component, caused by the propagation of shear waves,[17,18,30,41] and the steady component, which manifests with an effect similar to that of motion of a periodic array of spheres in a fluid medium. The unsteady component is dominant at short timescales, such as those corresponding to nondiffusive Brownian motion or high-frequency oscillatory motion. At these short timescales, the penetration depth of shear waves can be greater than the distance between the probe particle and its periodic neighbors (i.e., the simulation box length) and thus, can travel across the boundaries (Figure 1). One approach for avoiding these unsteady effects would be to use a larger simulation box, which would lead to a substantial increase in computational time. Without proper accounting for these unsteady effects, the highest frequency at which the PRST can be used will be limited.

The steady component, as mentioned earlier, can cause an effect similar to that in the creeping flow with PBC problem, a situation studied previously.[42–44] It was shown that in this case, the friction force experienced by a single particle in the array can be described using a modified Stokes' law as follows:

$$F = 6K\pi R\eta v, \quad (4)$$

where K is a correction parameter that is a function of the problem geometry. However, such a correction cannot be directly applied to the MD simulation since it was derived based on the particle being the frame of reference. In the MD simulations, the frame of reference is that of net zero momentum. A recent study by Ethier et al.[14] takes this into account and proposes a hydrodynamic correction factor, which can be applied to the viscosity derived from either the Stokes' law or SE relation, as follows:

$$\eta_H = \left(K_S \frac{f_v}{f_m}\right)^{-1} \eta, \quad (5)$$

where η_H is the modified viscosity, f_v is the fluid volume fraction, f_m is the fluid mass fraction, and K_S is a geometry-dependent factor as follows:

$$K_s{}^{-1} = 1 - 1.7601\phi^{\frac{1}{3}} + \phi - 1.5593\phi^2 + 3.9799\phi^{\frac{8}{3}} - 3.0734\phi^{\frac{10}{3}}, \quad (6)$$

Where ϕ is the particle(s) volume fraction. Equations (1) and (2) can then be used in conjunction with Equations (5) and (6) to calculate the correct viscosities from the simulations of probe particle motion. In each simulation, the viscosity is first calculated from either Equation (1) or Equation (2), depending on whether the technique is implemented in passive or active mode. Then, the geometry-dependent factor K_s is calculated using Equation (6). Finally, the correction factor is applied to the obtained viscosities via Equation (5).

2.3 | Model details

Four simple liquids with and without various functional groups were used in this study: acetone ($(CH_3)_2CO$), butanone ($CH_3C(O)CH_2CH_3$), decane ($C_{10}H_{22}$), and diethyl ether ($(C_2H_5)_2O$). These liquids were chosen because they are organic liquids with a variety of different functional groups, and their calculated viscosities when using the periodic perturbation method[45] reasonably matched the experimentally measured values. Two sets of five replicas of each system were made: one set of the "pure" systems (systems with no probe particles) and one set containing a probe particle. Each replica was made by equilibrating the system using different randomized initial velocities. The optimized potential for liquid simulations (OPLS) force field[46–48] was used throughout this study, and the ligpargen software[49] associated with the OPLS force field was used to obtain the initial structures of the aforementioned molecules using the 1.14*CM1A-LBCC charge model. The probe particle was made by cutting a sphere with a nominal radius of 10 Å from an FCC lattice made from neutral carbon atoms with $\sigma = 3.55$ Å and $\varepsilon = 0.076 \frac{kcal}{mol}$. The lattice spacing was set to be the same as the carbon atom's diameter (3.55 Å). Harmonic bonds with an equilibrium length of 1.34 Å and a bond stiffness of $549 \frac{kcal}{mol\,Å^2}$ were used to connect neighboring pairs of carbon atoms on the lattice together. These parameters correspond to those for a typical C–C bond and were obtained from the OPLS force field. The probe particle R_g was monitored during all the simulation runs to ensure that the particle did not become deformed.

In each system containing the probe, the interaction strength between the ith probe particle bead and jth atom of the fluid (ε_{ij}) was scaled by a factor of α, that is, $\varepsilon_{ij} = \alpha\varepsilon_{ij}{}^{mix}$, where $\varepsilon_{ij}{}^{mix} = \sqrt{\varepsilon_i \varepsilon_j}$. This means that the interaction strength between a carbon atom that is a part of the probe particle and other atoms in the medium would be stronger than the interactions between a carbon atom of the medium and other atoms in the medium by a factor of α. Six different values of α were used in this work: 1, 2, 3, 5, 8, and 10. Each system with a different scaling factor was equilibrated independently, resulting in 24 different sets of systems.

The nonbonded van der Waals and the electrostatic interactions were explicitly calculated within a cut-off distance of 12 Å. Beyond these cut-off distances, the interactions were handled by applying tail-corrections for the nonbonded van der Waals interactions and the particle-particle particle-mesh method[50,51] (with a tolerance of 1×10^{-4}) for the electrostatic interactions. All the simulations were performed using the LAMMPS software package.[52] The simulations were carried out either in the isothermal-isobaric ensemble (constant NPT, for equilibration) or the canonical ensemble (constant NVT, for production) with a pressure of 1 atm, a temperature of 298 K, and a time step of 1 fs. Nose–Hoover thermostat[53] and barostat[54] were used to regulate the temperature and pressure, with constants of 100 fs and 1 ps, respectively. All systems were equilibrated for a duration of 250 ps.

2.4 | Periodic perturbation method

The viscosities of the pure systems were obtained using the periodic perturbation method,[45] which serves as a frame of reference to compare the results obtained from the PRST. Experimental results were not used for validation because the viscosity results obtained from a simulation depend not only on the employed method but also on the force field. For example, the viscosity of water obtained from simulations using the periodic perturbation technique was much closer to the experimental value when the TIP5P and SPC/E water models were used compared with other water models (SPC, TIP3P, and TIP4P).[55] Here, we are not trying to evaluate the force-field, but the method. Therefore, we opt to compare the results of our simulations with results obtained from a different simulation technique rather than those obtained experimentally to eliminate any error arising from force field parameterization.

In the periodic perturbation method, the system is subjected to a periodic acceleration as follows[45]:

$$a_x(z) = A\cos\left(\frac{2\pi z}{l_z}\right), \quad (7)$$

where $a_x(z)$ is the acceleration imposed on each atom in the x direction based on its z coordinate, A is the acceleration amplitude,

TABLE 1 Viscosities of the four different simple fluids of interest obtained from the periodic perturbation (η), the standard error for those values (SE) as well as viscosities reported in the literature ($\eta_{Exp.}$).

Fluid	η (cP)	SE	$\eta_{Exp.}$ (cP)
Acetone	0.437	0.009	0.32 (at 20°C)[56]
Butanone	0.603	0.030	0.4 (at 25°C)[57]
Decane	1.161	0.038	0.85 (at 25°C)[58]
Diethyl ether	0.315	0.005	0.25 (at 20°C)[59]

and l_z is the simulation box length in the z-direction. At steady state, the acceleration results in a velocity profile as follows:

$$v_x(z) = V\cos\left(\frac{2\pi z}{l_z}\right). \tag{8}$$

The velocity amplitude V and the viscosity η are related to each other as follows:

$$V = \frac{A\rho}{\eta}\left(\frac{l_z}{2\pi}\right)^2 \tag{9}$$

and the resulting velocity profile is measured. The inverse viscosity is then calculated from the velocity amplitude in the steady state. All the periodic perturbations simulations were conducted for a duration of 200 ps with an acceleration amplitude of $1e^{-7}\frac{\text{Å}}{\text{fs}}$ at a temperature of 298 K and a pressure of 1 atm.

3 | RESULTS AND DISCUSSION

3.1 | Viscosity from the periodic perturbation method

The obtained viscosities of the four simple fluids from the periodic perturbation method and experiments are presented in Table 1.

The results obtained from the periodic perturbation method seem to be overestimating the viscosity when compared with those obtained from experiments. As mentioned earlier, the discrepancy between the simulation and experimental results can be caused by not just the method employed but also the force field used. Therefore, we will compare the results obtained from our probe rheology simulations with those obtained from the periodic perturbation method to eliminate any discrepancy caused by the force field.

3.2 | Probe particle hydrodynamic radius

The R_Hs of the probe particles were obtained as the position of the first solvation shell in the particle-fluid $g(r)$ plot. The $g(r)$ for various values of α for systems with acetone is shown in Figure 2. The same results for the rest of the systems are shown in Figure S1.

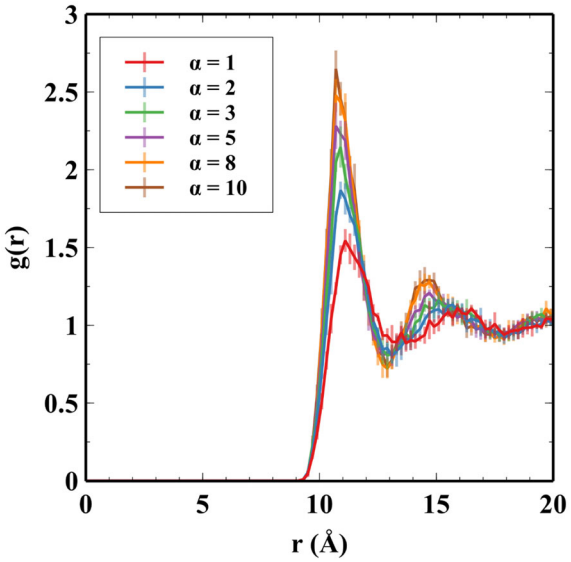

FIGURE 2 Plot of radial distribution function ($g(r)$) between the particle center-of-mass and fluid atoms for acetone versus distance from the probe particle's center-of-mass (r) for α equal to 1 (red), 2 (blue), 3 (green), 5 (purple), 8 (orange), and 10 (brown). The transparent vertical lines represent the statistical error.

As observed in Figures 2 and S1, the R_H slightly decreases (from ~11.3 to ~10.7 Å) as α increases, which is expected since a higher α translates to stronger particle-fluid interactions, thus the solvent particles are expected to be closer to the probe particle. Moreover, the height of the second peak also increases with the increasing α, which would also suggest a tighter packing of the fluid atoms around the probe particle as a result of increased probe-fluid interactions. For each system, the R_H was averaged across five replicas.

3.3 | Viscosity from the Brownian motion of the probe particle (passive mode)

The probe particle was allowed to undergo Brownian motion for a duration of 10 ns, thus ensuring that all particles exhibit a true diffusive motion, that is, the slope in the log–log plot of $\langle \Delta r^2 \rangle$ (mean-square displacement) versus t (time) reached 1. In all cases, 1 ns of simulation time is enough to observe the probe particle reaching the fully diffusive motion. A representative movie of the probe particle undergoing Brownian motion in diethyl ether can be found in the Supporting Information. The plots do not exhibit the ballistic motion at short times, since capturing this regime requires employing smaller timesteps. We did not opt to use such smaller timescales as the ballistic regime is not of interest in this work. The $\langle \Delta r^2 \rangle$ results for all values of α are shown in Figure 3 for systems with acetone. The results for the rest of the systems are shown in Figure S2.

As observed in Figure 3, the overall $\langle \Delta r^2 \rangle$ of the probe particle decreases with increasing α due to a decrease in the overall mobility of the probe particle as a result of increased particle-fluid interactions. The diffusion coefficients (D) of the embedded probe particles were obtained from a fit to $\langle \Delta r_b^2 \rangle$ as $\langle \Delta r^2 \rangle = 6Dt^n$ with $n = 1$ in the diffusive

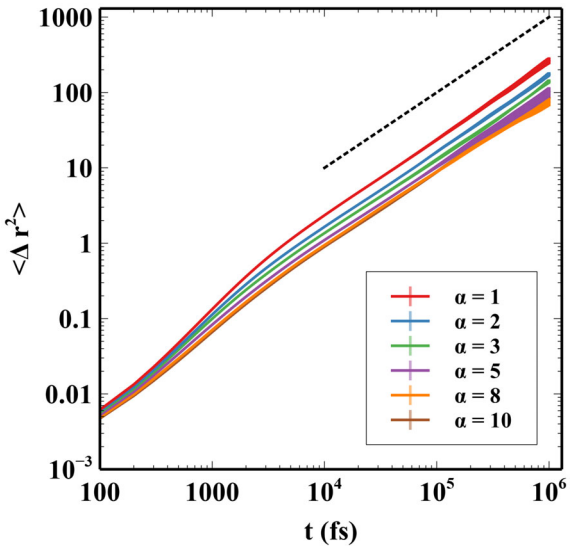

FIGURE 3 Log–log plot of mean-square displacement ($\langle \Delta r^2 \rangle$) versus time ($t$) for α equal to 1 (red), 2 (blue), 3 (green), 5 (purple), 8 (orange), and 10 (brown). The black dashed line represents a slope of 1 on the log–log plot.

regime. The values of D versus α are shown in Figure 4A for all the systems. The values of the diffusion coefficients were used in conjunction with Equation (1) and Equations (5) and (6) to calculate the viscosity of the surrounding fluid. The obtained normalized viscosities (η_n, the viscosities obtained from the motion of the probe particle divided by those obtained from the periodic perturbation method) versus α for all the systems are shown in Figure 4B.

As observed in Figure 4B, considering all the systems, a value of $\alpha = 2$ results in the η_n being closest to 1, thus matching the periodic perturbation results. Increasing the α beyond this value hinders the mobility of the probe particle undergoing Brownian motion too far. Increasing the probe-medium interaction strength results in an increase in the normal and tangential forces experienced by the probe particle, which increases the hydrodynamic friction force, manifesting in an increase in the viscosity observed by the probe particle and thus, a decrease in its mobility. Such a decrease in mobility seems to be more significant in decane than the other fluids since decane is the most viscous of those chosen for this study.

3.4 | Viscosity from the steady forced motion of the probe particle (active mode)

In these simulations, a constant force of varying amplitudes (5, 8, 10, 15, 20, 25, 40, and 50 $^{kcal}/_{mol\,Å}$ or 0.3475, 0.556, 0.695, 1.0425, 1.39, 1.3755, 2.78, and 3.475 nN) was applied to the probe particle in the z-direction for a duration of 50 ps. The magnitude of the Brownian force can be approximated as $\frac{k_B T}{R_H}$, which for a probe particle with an average hydrodynamic radius of 11 Å, will be about 3.7 pN. The amplitude of the constant driving force thus was chosen so that the effect of the Brownian force would be negligible compared with it. The probe particle was tethered to a spring in x and y directions with a stiffness of 100 $^{kcal}/_{mol\,Å^2}$ to limit the probe particle's center-of-mass displacement in those two directions to less than 1 Å. This tethering force does not affect the viscosity calculation since it does not have any component in the direction of probe particle motion but is necessary to limit the probe particle motion to only one direction. The probe particle velocity (v) was obtained from the slope of displacement of the probe particle's center-of-mass versus time and used in Equation (2) in conjunction with Equations (5) and (6) to calculate the viscosity of the surrounding fluid. The normalized viscosities are plotted as a function of the force amplitude (F) for different values of α for systems with acetone in Figure 5A. The same results for the rest of the systems are shown in Figure S3.

As observed in Figure 5A, the viscosity probed by the moving particle decreases when F, and consequently, the probe particle velocity, is increased. This is due to the inertial effects becoming significant at higher velocities, as evident from the increase in Reynolds number (Re) with increasing F (The values of Re as a function of F for different values of α and for systems with acetone are plotted in Figure 5B, and similar results for the rest of the systems are presented in Figure S4). The increase in Re with increasing F becomes less significant for higher values of α. This is an effect similar to that observed in Figure 2. The overall increase in the probe-fluid interaction (achieved by increasing α) results in a decrease in the overall mobility of the probe particle, which manifests as a decrease in the v.

It must be noted that the Stokes law is only valid at low Re, that is, $Re << 1$. Ideally, the Re should be as close to zero as possible. Practically, a difference of two orders of magnitude should be sufficient.[15] Thus, we only find the viscosities from cases for which $Re < 0.01$ acceptable. The normalized viscosities of the acceptable cases are plotted in Figure 6 for systems with acetone, and in Figure S5 for the rest of the systems.

As evident from Figure 6, the number of acceptable cases increases with increasing α, as a result of the interplay between Re and α, since an increase in the strength of the particle-fluid interactions (i.e., increase in α) results in a decrease in the overall mobility of the probe particle (i.e., decrease in v and consequently, in Re). Finally, it must be noted that the motion of the probe particle induces shear in the fluid (with an effective shear rate of $\dot{\gamma} = \frac{v}{R}$). Thus, the obtained viscosities cannot be considered zero-shear viscosity. Instead, the zero-shear viscosity can be obtained from the plateau of the viscosity versus $\dot{\gamma}$ (effectively F) plot. However, the number of acceptable cases for a given value of α can be too low (especially when $\alpha = 1$). Therefore, we find the zero-shear viscosity by extrapolating the acceptable results at the limit of $\dot{\gamma} \to 0$. This is done via a linear fit to the normalized viscosity versus F data (dashed lines in Figure 6). The linear fit provided the best fit to the results across all cases. The final normalized viscosities, obtained from both the passive and active modes, as a function of α for all the fluids are presented in Figure 7. The results obtained from the passive mode are presented again for comparison.

As evident from Figure 7, the normalized viscosities are closest to a value of 1 when $\alpha = 2$, from both active and passive modes. For $\alpha = 2$, the obtained viscosities from our method are less than 10% different than those obtained from the periodic perturbation method, except in the case of decane in active mode, for which the difference is

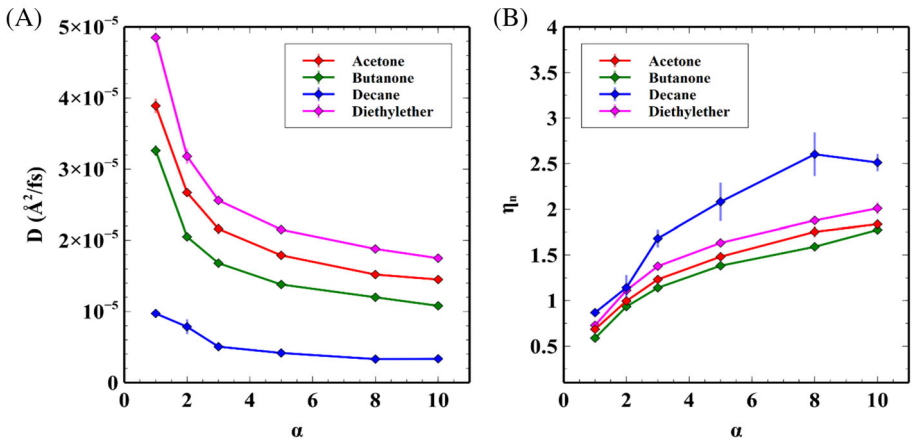

FIGURE 4 Plot of (A) diffusion coefficient (D) and (B) normalized viscosity (η_n) versus α for systems with acetone (red), decane (blue), butanone (green), and diethyl ether (pink). The vertical transparent lines represent the standard error.

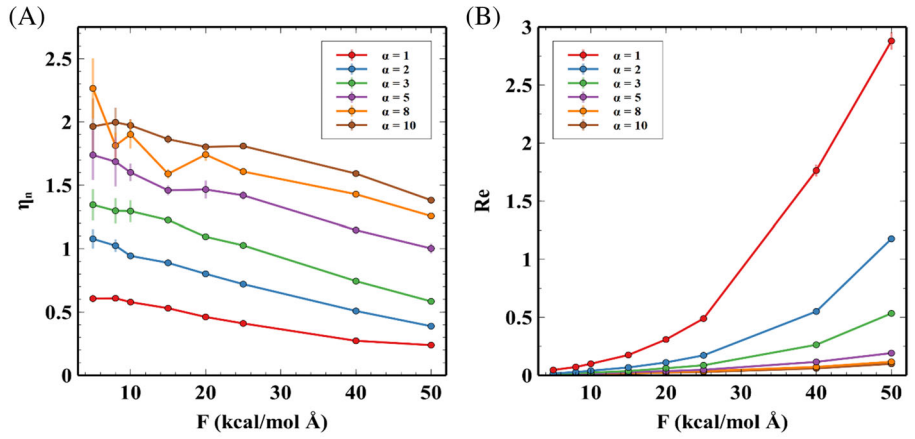

FIGURE 5 Plot of (A) normalized viscosity (η_n) and (B) Reynolds number (Re) versus the amplitude of the applied force (F) for α equal to 1 (red), 2 (blue), 3 (green), 5 (purple), 8 (orange), and 10 (brown). The transparent vertical lines represent the statistical error.

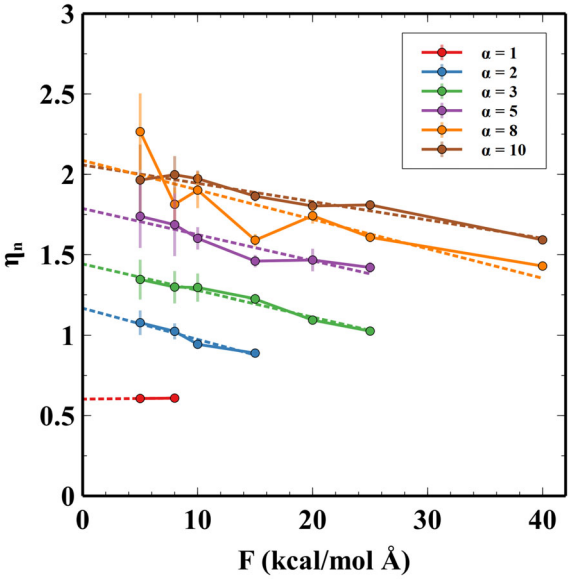

FIGURE 6 Plot of normalized viscosity (η_n) for cases in which $Re < 0.01$ versus the amplitude of the applied force (F) for α equal to 1 (red), 2 (blue), 3 (green), 5 (purple), 8 (orange), and 10 (brown). The dashed lines represent linear fits to the data. The transparent vertical lines represent the statistical error.

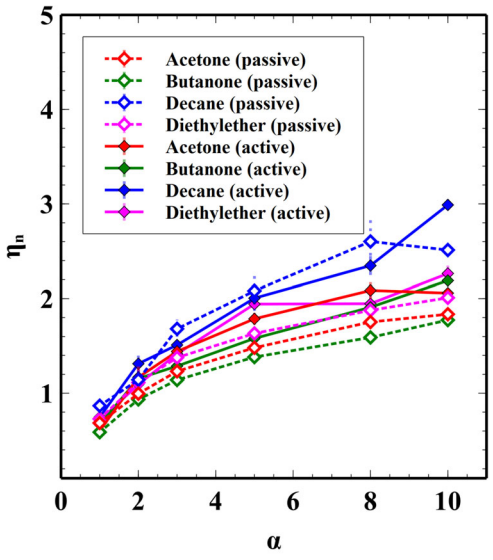

FIGURE 7 Plot of normalized viscosity (η_n) versus α for systems with acetone (red), decane (blue), butanone (green), and diethyl ether (pink). The solid lines and filled markers correspond to results obtained from the active mode, and the dashed lines and hollow markers correspond to results obtained from the passive mode. The vertical transparent lines represent the standard error.

$\sim 30\%$. This variance falls in the typical range of variance among different methods for calculating viscosity in MD simulations. For example, using both an equilibrium and a nonequilibrium approach (GK and NEMD, respectively), the viscosity of water at 303.15 K was found to be 0.62 ± 0.04 cp and 0.66 ± 0.08 cp, respectively, using the SPC/E water model.[60] Using the same water model, the viscosity of water at 300 K was found to be 0.722 ± 0.006 cp using the periodic perturbation method.[55] For reference, the viscosity of water at a temperature of 303.15 K is 0.7972 cp.

Similar results were found for CG simulations where LJ fluids[30,31] unentangled[17,18] and weakly entangled[14,15] coarse-grained polymer melts, all required interactions between the particle and the fluid to be twice as high as fluid–fluid interactions. Furthermore, the overestimation of viscosity when the probe-medium interaction strength is too high and its underestimation when the probe-medium interaction is too weak, as demonstrated in Figures 6 and 7, were similarly seen for simulations of an LJ fluid.[30] Thus, the successful implementation of our model in the atomistically detailed simulations is consistent with previous implementations of PRST in coarse-grained simulations concerning the strength of probe-medium interactions required to obtain accurate results relative to that of medium-medium.

The agreement between the results obtained from the passive and active modes for four different liquids indicates that the proposed model is universal regardless of the application mode and can work in organic fluids. The fact that both CG and atomistically detailed models (including LJ fluids and polymer melts in the case of CG) produced the best results when probe-fluid interactions are twice that of the dominant fluid–fluid interactions suggests that such a modification should be universal for PRST.

For all the four organic liquids studied in this work, the most prevalent atom type in the system, besides hydrogen, is carbon. Hydrogen-specific interactions are frequently ignored without any significant loss of accuracy in simulations, as demonstrated by the success of united-atom force-fields in predicting different properties of various organic materials, from simple olefins[61] to proteins.[62] Therefore, the most prevalent important interaction type in these systems is carbon–carbon. For other organic fluids, a similar α may be acceptable, but for aqueous fluids, or more exotic fluids, scaling the particle-fluid interaction by the dominant fluid–fluid interaction may be beneficial. Setting the probe-medium interaction to be twice as strong as the dominant fluid–fluid nonbonded interaction should serve as a reasonable initial guess for tuning the probe-medium interactions in fluids with more complex interactions.

PRST has the advantage of better performance than NEMD in terms of CPU time,[14] and its capability to probe location variations in mechanical properties. While PRST does have disadvantages, such as having to extrapolate to $\dot{\gamma} \to 0$, this work provides guidelines for parameter selection in atomistic models, allowing PRST to be used in a wider variety of cases.

4 | CONCLUSIONS

In this work, the viscosities of four different simple fluids in atomistically detailed MD simulations were obtained using PRST in passive and active modes (i.e., from both Brownian and forced motion, respectively). The rough probe particles are made up of a collection of neutral carbon atoms, loosely based on a diamond nanoparticle. The strength of the particle-fluid interactions was tuned by scaling the interaction strength parameter ε by a factor of α.

In passive mode, the diffusion coefficient of the probe particle when its Brownian motion was in the diffusive regime was calculated and used in conjunction with the SE relation to obtain the viscosities. Furthermore, the obtained viscosities were adjusted by a hydrodynamic correction factor to account for the effects of the AHIs on the motion of the probe particle, which arises from the use of PBCs in the simulations. When the particle-fluid interactions are scaled by a factor of 2, these viscosities are consistent with other accepted techniques.

In the active mode, the probe particle was dragged through the medium under a constant applied force of various amplitudes. When (1) the applied force is large enough (i.e., two orders of magnitude large than the Brownian force), (2) the simulation is run long enough to achieve constant velocity (longer than 1 ns here), (3) the Reynold number is relatively small (i.e., $Re < 0.01$), and (4) the interaction between the particle and the fluid is scaled by a factor of 2 to ensure the no-slip boundary condition, the zero-shear viscosities are in good agreement with other accepted techniques.

The results obtained from both passive and active modes are in agreement, and both modes produce the most accurate results for the case where the probe-medium interaction strength is twice as high as that of the medium-medium, which is consistent with the previous implementation of the PRST in coarse-grained simulations. Furthermore, the variance in our results, from both active and passive modes, is within the typical range of variance among various viscosity calculation methods in MD simulations such as the GK approach, NEDM and periodic perturbation. Moreover, a trend of overestimation when the probe-medium interactions are too strong is also observed, consistent with previous literature observations.

The most interesting advantage of the probe rheology simulations compared with other methods such as NEMD is indeed its capability to probe local variations in mechanical properties that can arise from a variety of factors such as structural or dynamic heterogeneities. Such an advantage is not demonstrated in this work since it is not the main purpose of this study. In this work, instead of performing atomistically detailed probe rheology on complex systems that can exhibit such heterogeneities, we have instead chosen to calibrate the parameters for the atomistically detailed representation of a probe particle in simulations of simple fluids. Calibrating force field parameters in systems where variations in the system can affect mechanical properties in addition to force field parameters is simply not practical. The proposed model for implementing the PRST in atomistically detailed simulations using an interaction scaling factor of 2 seems to be universal and applicable to a wide range of compounds. Thus, these results can now be used to explore and demonstrate the broader applicability of the model and its unique capability to probe the local mechanical properties of complex materials, such as TSMPs, in atomistically detailed simulations in future works.

ACKNOWLEDGMENTS

The funding for this work is provided by the US National Science Foundation under grant number OIA-1946231 and the Louisiana Board of Regents for the Louisiana Materials Design Alliance (LAMDA). Additional funding was provided via the Louisiana Board of Regents through LEQSF-EPS(2022)-LAMDA-Seed-Track-1C-06. The high-performance computing resources provided by the Louisiana Optical Network Infrastructure (LONI) were used to conduct all the simulations.

DATA AVAILABILITY STATEMENT

The data that support the findings of this study are available from the corresponding author upon reasonable request.

ORCID

Pouria Nourian https://orcid.org/0000-0001-5270-7639

Andrew J. Peters https://orcid.org/0000-0001-5031-2828

REFERENCES

[1] E. M. Furst, *Curr. Opin. Colloid Interface Sci.* **2005**, *10*(1–2), 79.
[2] E. M. Furst, T. M. Squires, *Microrheology*, Oxford University Press, Oxford **2017**.
[3] Y. Kimura, *J. Phys. Soc. Jpn.* **2009**, *78*(4), 041005.
[4] A. Mukhopadhyay, S. Granick, *Curr. Opin. Colloid Interface Sci.* **2001**, *6*(5–6), 423.
[5] T. M. Squires, T. G. Mason, *Annu. Rev. Fluid Mech.* **2010**, *42*, 413.
[6] T. A. Waigh, *Rep. Prog. Phys.* **2005**, *68*(3), 685.
[7] D. Weihs, T. G. Mason, M. A. Teitell, *Biophys. J.* **2006**, *91*(11), 4296.
[8] S. Yamada, D. Wirtz, S. C. Kuo, *Biophys. J.* **2000**, *78*(4), 1736.
[9] F. Ould-Kaddour, D. Levesque, *Phys. Rev. E* **2000**, *63*(1), 011205.
[10] J. Liu, D. Cao, L. Zhang, *J. Phys. Chem. C* **2008**, *112*(17), 6653.
[11] M. Vergeles, P. Keblinski, J. Koplik, J. R. Banavar, *Phys. Rev. E* **1996**, *53*(5), 4852.
[12] J. Schmidt, J. Skinner, *J. Phys. Chem. B* **2004**, *108*(21), 6767.
[13] J. Schmidt, J. Skinner, *J. Chem. Phys.* **2003**, *119*(15), 8062.
[14] J. G. Ethier, P. Nourian, R. Islam, R. Khare, J. D. Schieber, *J. Rheol.* **2021**, *65*(6), 1255.
[15] P. Nourian, R. Islam, R. Khare, *J. Rheol.* **2021**, *65*(4), 617.
[16] M. Vergeles, P. Keblinski, J. Koplik, J. R. Banavar, *Phys. Rev. Lett.* **1995**, *75*(2), 232.
[17] M. Karim, T. Indei, J. D. Schieber, R. Khare, *Phys. Rev. E* **2016**, *93*(1), 012501.
[18] M. Karim, S. C. Kohale, T. Indei, J. D. Schieber, R. Khare, *Phys. Rev. E* **2012**, *86*(5), 051501.
[19] T. Ge, G. S. Grest, M. Rubinstein, *Phys. Rev. Lett.* **2018**, *120*(5), 057801.
[20] L. Onsager, *Phys. Rev.* **1931**, *37*(4), 405.
[21] M. S. Green, *J. Chem. Phys.* **1954**, *22*(3), 398.
[22] R. Kubo, *J. Phys. Soc. Jpn.* **1957**, *12*(6), 570.
[23] Y. Zhang, A. Otani, E. J. Maginn, *J. Chem. Theory Comput.* **2015**, *11*(8), 3537.
[24] D. J. Evans, G. Morriss, *Phys. Rev. A* **1984**, *30*(3), 1528.
[25] B. D. Todd, P. J. Daivis, *Nonequilibrium Molecular Dynamics: Theory, Algorithms and Applications*, Cambridge University Press, Cambridge **2017**.
[26] C. D. Wick, A. J. Peters, G. Li, *Polymer* **2021**, *213*, 123319.
[27] C. Liu, H. Qin, P. Mather, *J. Mater. Chem.* **2007**, *17*(16), 1543.
[28] F. Xie, L. Huang, J. Leng, Y. Liu, *J. Intell. Mater. Syst. Struct.* **2016**, *27*(18), 2433.
[29] C. Lindemann, R. Rikmenspoel, *J. Phys. E: Sci. Instrum.* **1972**, *5*(2), 178.
[30] S. C. Kohale, R. Khare, *J. Chem. Phys.* **2008**, *129*(16), 164706.
[31] S. C. Kohale, R. Khare, *J. Chem. Phys.* **2010**, *132*(23), 234706.
[32] R. Poling-Skutvik, R. Krishnamoorti, J. C. Conrad, *ACS Macro Lett.* **2015**, *4*(10), 1169.
[33] I. Kohli, A. Mukhopadhyay, *Macromolecules* **2012**, *45*(15), 6143.
[34] C. D. Chapman, K. Lee, D. Henze, D. E. Smith, R. M. Robertson-Anderson, *Macromolecules* **2014**, *47*(3), 1181.
[35] N. Ziębacz, S. A. Wieczorek, T. Kalwarczyk, M. Fiałkowski, R. Hołyst, *Soft Matter* **2011**, *7*(16), 7181.
[36] A. Tuteja, M. E. Mackay, S. Narayanan, S. Asokan, M. S. Wong, *Nano Lett.* **2007**, *7*(5), 1276.
[37] J. T. Kalathi, U. Yamamoto, K. S. Schweizer, G. S. Grest, S. K. Kumar, *Phys. Rev. Lett.* **2014**, *112*(10), 108301.
[38] V. Ganesan, V. Pryamitsyn, M. Surve, B. Narayanan, *J. Chem. Phys.* **2006**, *124*, 221102.
[39] A. Karatrantos, R. J. Composto, K. I. Winey, N. Clarke, *J. Chem. Phys.* **2017**, *146*(20), 203331.
[40] R. Walser, A. E. Mark, W. F. van Gunsteren, *Chem. Phys. Lett.* **1999**, *303*(5–6), 583.
[41] T. Indei, J. D. Schieber, A. Córdoba, *Phys. Rev. E* **2012**, *85*(4), 041504.
[42] H. Hasimoto, *J. Fluid Mech.* **1959**, *5*(2), 317.
[43] A. S. Sangani, A. Acrivos, *Int. J. Multiphase Flow* **1982**, *8*(3), 193.
[44] A. Zick, G. Homsy, *J. Fluid Mech.* **1982**, *115*, 13.
[45] B. Hess, *J. Chem. Phys.* **2002**, *116*(1), 209.
[46] W. L. Jorgensen, J. Tirado-Rives, *J. Am. Chem. Soc.* **1988**, *110*(6), 1657.
[47] W. L. Jorgensen, J. D. Madura, C. J. Swenson, *J. Am. Chem. Soc.* **1984**, *106*(22), 6638.
[48] W. L. Jorgensen, D. S. Maxwell, J. Tirado-Rives, *J. Am. Chem. Soc.* **1996**, *118*(45), 11225.
[49] L. S. Dodda, I. Cabeza de Vaca, J. Tirado-Rives, W. L. Jorgensen, *Nucleic Acids Res.* **2017**, *45*(W1), W331.
[50] M. P. Allen, D. J. Tildesley, *Computer Simulation of Liquids*, Oxford University Press., Oxford **2017**.
[51] R. W. Hockney, J. W. Eastwood, *Computer Simulation Using Particles*, CRC Press, Boca Raton **1988**.
[52] S. Plimpton, *J. Comput. Phys.* **1995**, *117*(1), 1.
[53] M. Parrinello, A. Rahman, *J. Appl. Phys.* **1981**, *52*(12), 7182.
[54] W. Shinoda, M. Shiga, M. Mikami, *Phys. Rev. B* **2004**, *69*(13), 134103.
[55] Y. Song, L. L. Dai, *Mol. Simul.* **2010**, *36*(7–8), 560.
[56] D. R. Gustafson, *Physics: Health and the Human Body*, Wadsworth Publishing Company, Belmont **1980**.
[57] R. A. Lewis, *Hawley's Condensed Chemical Dictionary*, John Wiley & Sons, Hoboken **2016**.
[58] J. Dymond, H. O/ye, *J. Phys. Chem. Ref. Data* **1994**, *23*(1), 41.
[59] J. G. Speight, *Lange's Handbook of Chemistry*, Vol. 1, McGraw-Hill, New York **2005**.
[60] S. Balasubramanian, C. J. Mundy, M. L. Klein, *J. Chem. Phys.* **1996**, *105*(24), 11190.
[61] S. K. Nath, B. J. Banaszak, J. J. de Pablo, *J. Chem. Phys.* **2001**, *114*(8), 3612.
[62] L. Yang, C. H. Tan, M. J. Hsieh, J. Wang, Y. Duan, P. Cieplak, J. Caldwell, P. A. Kollman, R. Luo, *J. Phys. Chem. B* **2006**, *110*(26), 13166.

SUPPORTING INFORMATION

Additional supporting information can be found online in the Supporting Information section at the end of this article.

How to cite this article: P. Nourian, A. J. Peters, *J. Comput. Chem.* **2023**, 1. https://doi.org/10.1002/jcc.27099